Nyrow, A., Sternemann, C., Wilke, M., Gordon, R. A., Mende, K., Yavaş, H., Simonelli, L., Hiraoka, N., Sahle, C. J., Huotari, S., Andreozzi, G. B., Woodland, A. B., Tolan, M., Tse, J. S. (2014): Iron speciation in minerals and glasses probed by M2/3-edge X-ray Raman scattering spectroscopy. - *Contributions to Mineralogy and Petrology*, *167*, 5

DOI: http://doi.org/10.1007/s00410-014-1012-8

**Contributions to Mineralogy and Petrology manuscript No.**
(will be inserted by the editor)

# Iron speciation in minerals and glasses probed by $M_{2/3}$-edge x-ray Raman scattering spectroscopy

**A. Nyrow · C. Sternemann · M. Wilke · R. A. Gordon · K. Mende · H. Yavaş · L. Simonelli · N. Hiraoka · Ch. J. Sahle · S. Huotari · G. B. Andreozzi · A. B. Woodland · M. Tolan · J. S. Tse**

Received: date / Accepted: date

**Abstract** We present a spectroscopic study of the iron $M_{2/3}$-edge for several minerals and compounds to reveal information about the oxidation state and the local coordination of iron. We describe a novel approach to probe the iron $M_{2/3}$-edge bulk sensitively using x-ray Raman scattering. Significant changes in the onset and shape of the Fe $M_{2/3}$-edge were observed on ferrous and ferric model compounds with Fe in octahedral and tetrahedral coordination. Simulation of the spectra is possible using an atomic multiplet code, which potentially allows determination of e.g. crystal field parameters in a quantitative manner. A protocol is discussed that allows for determination of the Fe oxidation state in compounds by linear combination of spectra of ferric and ferrous end-members. The presented results demonstrate the capabilities of Fe $M_{2/3}$-edge spectroscopy by x-ray Raman scattering to extract information on the ratio of trivalent to total iron $Fe^{3+}/\sum Fe$ and local coordination. As x-ray Raman scattering is performed with hard x-rays, this approach is suitable for in-situ experiments at high pressure and temperature. It thus may provide indispensable information on oxidation state, electronic structure and local structure of materials that are important for physical and chemical processes of the deep Earth.

**Keywords** Iron speciation · minerals · x-ray scattering · x-ray absorption spectroscopy

**PACS** 61.05.cf · 78.70.Dm · 91.60.-x

A. Nyrow, C. Sternemann, K. Mende and M. Tolan
Fakultät Physik / DELTA, Technische Universität Dortmund, Dortmund, D-44221, Germany
E-mail: alexander.nyrow@tu-dortmund.de; christian.sternemann@tu-dortmund.de

M. Wilke
Deutsches GeoForschungsZentrum, Section 3.3, Potsdam, D-14473, Germany

R. A. Gordon
PNCSRF, APS Sector 20, Argonne, IL, USA 60439

H. Yavaş
Photon Science at DESY, D-22607 Hamburg, Germany

L. Simonelli
European Synchrotron Radiation Facility, Grenoble Cedex, F-38043, France *Present address: CELLS - ALBA Synchrotron Light Facility, Barcelona, Spain*

N. Hiraoka
National Synchrotron Radiation Research Center, Hsinchu 30076, Taiwan

Ch. J. Sahle and S. Huotari
Department of Physics, P.O. Box 64, University of Helsinki, FI-00014 Helsinki, Finland

G. B. Andreozzi
Dipartimento di Scienze della Terra, Sapienza Università di Roma, I-00185 Rome, Italy

A. B. Woodland
Institut für Geowissenschaften, Universität Frankfurt, Altenhöferallee 1, D-60438 Frankfurt, Germany

J. S. Tse
Department of Physics and Engineering Physics, University of Saskatchewan, Saskatoon, Canada S7N 5E2

## 1 Introduction

Iron is the most abundant transition metal in the bulk Earth. It strongly influences the chemical and physical properties of iron-bearing minerals, glasses, and melts, which in turn affect many geological processes [Badro et al. (2003),Duffy (2008),Ono et al. (2007)]. At conditions of the deep Earth, the $Fe^{3+}/\sum Fe$ and the Fe coordination may vary dramatically, which is relevant for e.g. iron partitioning between Fe-Mg phases or behavior of iron during partial melting [Irifune and Isshiki (1998),

McCammon et al. (2004), Okuchi (1997), Smyth et al. (2005), Wilke et al. (1999), Zerr and Boehler (1993), Zerr and Boehler (1994)]. Consequently, detailed information on the structure and its dependence on chemical composition of iron-bearing compounds is required at high temperature and high pressure conditions to better constrain the thermodynamic conditions where relevant geological processes take place [Parkinson and Arculus (1997), Wood et al. (1989)].

Despite intense research during the last decades, quantitative determination of the oxidation and coordination state of iron in compounds of geological relevance is still a challenge under in-situ conditions. Mössbauer spectroscopy is widely used to investigate the oxidation state of iron in phases of relevance for geological, environmental and technological applications [Dunlap et al. (1998), Fierro et al. (2011), McCammon (1997), Mysen (1991), Pacella et al. (2012)]. However, this technique is demanding if applied to samples with low Fe content, which works only if they are enriched in $^{57}$Fe [Sobolev et al. (1999)]. For very small samples, a special radiation microsource is needed. X-ray absorption spectroscopy is another tool that is widely used for determining the Fe oxidation state. A typical such measurement would be that of the Fe K-edge, with emphasis on both edge position and pre-edge features shown to be sensitive to valence and coordination [Wilke et al. (2001), Westre et al. (1997)].

Studies of Fe-containing mineral specimens can be done for low Fe content and with high spatial resolution [Gauthier et al. (1999), Newville et al. (1999)] with excitation of the Fe K-edge under ambient conditions [Berry et al. (2010), Schmid et al. (2003), Munoz et al. (2006), Wilke et al. (2001)], but in-situ measurements (high pressure, temperature) of the pre-edge in diamond anvil cells (DACs) [Narygina et al. (2009), Wilke et al. (2006)] present a greater challenge to obtain data of similar quality as that which can be obtained under ambient conditions. Soft x-ray absorption (SXAS) [Crocombette et al. (1995), Heijboer et al. (2005), de Groot et al. (2010)] or electron energy loss spectroscopy (EELS) [Calvert et al. (2005), Cavé et al. (2006), Miot et al. (2009), Boulard et al. (2012), Tan et al. (2012), Bourdelle et al. (2013)] measurements of Fe $L_{2/3}$- (2p to d at 706.8 eV and 719.9 eV) and $M_{2/3}$-edges (3p to d at 52.7 eV) are complementary to the K-edge measurements, providing additional sensitivity to oxidation state and also to spin state. These experiments, however, require vacuum conditions and are more surface sensitive than the higher energy K-edge. The low-energy of the incident photons in the soft x-ray regime prohibits DAC methods. As discussed by van der Laan though [van der Laan (1991)], the M-edges are highly sensitive to spin state so it would be beneficial to be able to measure them on a more regular basis than has been done for materials of geological relevance [van Aken et al. (1999), Moreau et al. (2012), Xiong et al. (2012)].

In this paper we use non-resonant inelastic x-ray scattering, i.e. x-ray Raman scattering (XRS), in order to measure the iron $M_{2/3}$-edge, in a way similar to SXAS and EELS, but with high bulk sensitivity, which potentially allows for in-situ experiments at extreme conditions. The suitability of XRS for high pressure experiments has already been shown for various elements, e.g carbon [Mao et al. (2003)], boron [Lee et al. (2005)], oxygen [Lee et al. (2008), Sahle et al. (2013)], silicon [Sternemann et al. (2013), Tse et al. (2013)], barium [Tse et al. (2011)], or vanadium [Ding et al. (2014)]. We study synthetic samples of FeO, $Fe_2SiO_4$, $FeAl_2O_4$, $Fe_2O_3$, and $FePO_4$, which serve as key examples for iron-bearing minerals and compounds with different iron oxidation state and coordination. They are used as a framework for evaluating the information that can be obtained by this technique for Fe-bearing mineral phases that are important throughout the deep Earth, ranging from Fe-Ni alloys of the Earth's core [Antonangeli et al. (2010), Lin et al. (2010), Terasaki et al. (2011)] to Fe-Mg silicates in mantle [Fang and Ahuja (2008), Hofmeister (2006), Otsuka et al. (2010)] and crust, as well as extraterrestrial materials [Edwards et al. (2000), Xu and Lin (2000)].

First we give a short discussion on the theory of XRS spectroscopy followed by an overview on samples and experimental details. Then we demonstrate how XRS can be applied to measure dipole and multipole excitations and how the results can be compared to theory. Finally, we discuss in detail the sensitivity of XRS measurements to determine iron coordination and oxidation state and we use XRS to estimate the $Fe^{3+}/\sum Fe$ ratio of glasses synthesized at different redox conditions.

## 2 Theory of x-ray Raman scattering

The inelastic x-ray scattering process occurs when an incoming x-ray photon is scattered by the electrons of the sample system, leading to a partial transfer of its energy and momentum. The energy and momentum transfer result in different excitations, such as valence band excitations, Compton scattering or phonon excitations [Bergmann et al. (2004), Hämäläinen and Manninen (2001), Krisch and Sette (2002), Schülke (2007)]. Electronic excitations from a core state to a non-occupied state can occur if the transferred energy is in the vicinity of electron binding energies. Measuring those excitations allows for studies of absorption edges in both the dipole and the non-dipole limit. The technique that

exploits such phenomena is called non-resonant inelastic x-ray scattering or x-ray Raman scattering (XRS). Typically, the scattered photons are measured at fixed outgoing photon energy ( 6 - 20 keV) as the energy of the incident photons is scanned at energy-loss values in the vicinity of a certain absorption edge (e.g. 53 eV, 543 eV and 1071 eV for the iron M-, oxygen K- and sodium K- edge, respectively). In contrast to EELS or SXAS, XRS is highly bulk sensitive because the energy of the incoming and scattered photons is in the hard x-ray regime. The measured quantity in such an experiment is proportional to the dynamic structure factor, which is given by [Schülke (2007)]

$$S(\mathbf{q},\omega) \propto \sum_f \left|\langle \mathrm{f}| \sum_j e^{-i\mathbf{q}\cdot\mathbf{r}_j} |\mathrm{c}\rangle\right|^2 \delta(E_c - E_f + \hbar\omega). \quad (1)$$

For XRS the dynamic structure factor is proportional to the excitation probability from an initial core state $|\mathrm{c}\rangle$ with energy $E_c$ to all non-occupied final states $|\mathrm{f}\rangle$ with energy $\mathrm{E}_f$. The momentum transfer vector is $\mathbf{q}$ and the sum is taken over the electrons of the system with position $\mathbf{r}_j$. The delta-function ensures energy conservation with the energy transfer $\hbar\omega$.
The dynamic structure factor contains element selective information about the local chemical and electronic structure as can be seen if expressed in terms of the transition matrix $M_L(\mathbf{q}, E)$ and the partial non-occupied electronic density of states $\rho_L(E)$ with the angular momentum channel L: [Soininen et al. (2006)]

$$S(\mathbf{q},\omega) = \sum_L |M_L(\mathbf{q}, E)|^2 \rho_L(E). \quad (2)$$

According to equation (2) the weight of the matrix elements for different excitation channels (dipole and non-dipole) strongly changes with the magnitude of $q$ giving rise to dominating dipole contribution (e.g. 3p to 3d) for qr<<1 providing a signal similar to that obtained by SXAS and EELS. At higher $q$ increasing contributions of non-dipole excitations are observed. In an experiment $q$ can be easily tuned by a variation of the scattering angle $2\theta$ due to $q = \frac{4\pi}{\lambda} \sin(2\theta/2)$. Measurements performed at low and high $q$ reveal a more complete picture of the electronic density of states [Soininen et al. (2006), Bradley et al. (2011)]. The special properties of XRS have made it an indispensable tool to accomplish experimental challenges if soft x-rays and electrons cannot be applied as a probe, see e.g. [Gordon et al. (2008), Inkinen et al. (2013), Lee et al. (2005), Lee et al. (2008), Mao et al. (2003), Mattila et al. (2005), Sahle et al. (2013), Soininen et al. (2005), Sternemann et al. (2005), Sternemann et al. (2013), Tse et al. (2011), Tse et al. (2013)].

In the case of transition metals atomic excitations dominate the XRS M- and L-edge spectra [Gordon et al. (2009)]. In fact, the 3p hole and the 3d hole wave functions overlap significantly and the final states are found by the vector coupling of these two wave functions. This so-called multiplet effect is well known in atomic physics and can be observed also in solids. Here, it has to be used rather than the density-of-states approach discussed above. We express the dynamic structure factor via

$$S(\mathbf{q},\omega) = \sum_f \sum_{k=0}^{\infty} D_k \left|\langle \mathrm{f(r)}\, |j_k(qr)|\, \mathrm{c(r)}\rangle\right|^2 \times \delta(E_c - E_f + \hbar\omega) \quad (3)$$

with the spherical Bessel function $j_k(qr)$ of $k$-th order, which gives rise to the $q$-dependence, the radial wave functions f(r) and c(r), and coefficients $\mathrm{D}_k$ [Gordon et al. (2009)]. Since the initial state wave function ($3p$) is odd and the final $d$ wave function ($3d$) even in presence of inversion symmetry, only transitions of odd parity and $d - p = 1 \leq k \leq p + d = 3$ contribute in equation (3). Thus, only terms with $k = 1$ (dipole transitions) and $k = 3$ (octupole transitions) contribute to the XRS spectrum of the Fe $M_{2/3}$-edge [Haverkort et al. (2007)]. The relative weight of these two transitions is governed by the magnitude of the momentum transfer $q$. This approach will be used later to discuss the Fe $M_{2/3}$-edge spectra.

## 3 Sample description and experimental details

### 3.1 Samples

The sensitivity of the iron $M_{2/3}$-edge's shape regarding the iron oxidation state and local coordination was probed for synthetic crystalline compounds with $Fe^{2+}$ and $Fe^{3+}$ in octahedral and tetrahedral configuration. The momentum-transfer dependence of XRS spectra was investigated using FeO ($Fm3m$) and $\alpha$-$Fe_2O_3$ ($R\bar{3}c$, corresp. to hematite), whereas high-resolution XRS measurements were performed for synthetic $FeAl_2O_4$ ($Fd\bar{3}m$, corresp. to hercynite [Andreozzi and Lucchesi (2002)]), $Fe_2SiO_4$ ($Pbnm$, corresp. to fayalite), $FePO_4$ ($P3_121$, iron(III) phosphate with berlinite-structure ($AlPO_4$), corresp. to rodolicoite) and $\alpha$-$Fe_2O_3$ ($R\bar{3}c$). FeO and $Fe_2SiO_4$ have $Fe^{2+}$ in octahedral coordination, whereas $FeAl_2O_4$ contains $Fe^{2+}$ in tetrahedral coordination. $\alpha$-$Fe_2O_3$ and iron-(III)-phosphate have $Fe^{3+}$ in octahedral and tetrahedral coordination, respectively. FeO and $\alpha$-$Fe_2O_3$ powders with 99.9% and 99.995% trace metals basis, respectively, were purchased from Sigma Aldrich.

The $FeAl_2O_4$ sample was synthesized and characterized by [Andreozzi and Lucchesi (2002)]. The chemical analysis by electron microprobe (EMP) shows 44.7±0.2 wt.% $FeO_{tot}$ and 55.5±0.4 wt.% $Al_2O_3$. Stoichiometric calculation from the EMP analysis and Mössbauer spectroscopy revealed an $Fe^{2+}/\sum Fe$ ratio of 0.92 and 0.94, respectively, i.e. a small contribution of $Fe^{3+}$. In $FeAl_2O_4$ 85% $Fe^{2+}$ occurs in tetrahedral coordination whereas 15% $Fe^{2+}$ is octahedrally coordinated. $FePO_4$ and $Fe_2SiO_4$ were analyzed by Fe K-edge XANES using the method of [Wilke et al. (2001)]. $FePO_4$ (pre-edge centroid position at 7113.55±0.01 eV) did not show any contribution by $Fe^{2+}$ and $Fe_2SiO_4$ (pre-edge centroid position at 7111.96±0.02 eV) no $Fe^{3+}$. All used samples were characterized in addition by x-ray diffraction measurements at beamline BL9 [Krywka et al. (2007)] of the synchrotron radiation source DELTA (Dortmund, Germany) to verify sample structure and to exclude impurities. For XRS measurements, the powdered samples were pressed into pellets.

In addition to crystalline compounds, we measured three synthetic glasses to test potential for determining the $Fe^{3+}/\sum Fe$ ratio. Two glasses were used with a composition of a transitional alkalic basalt from Iceland [Thy and Lofgren (1994)], RB0-1 and RB0-4, that were synthesized at 1350°C at two different oxygen fugacities and characterized by EMP, wet chemical analysis and Mössbauer spectroscopy, c.f. [Wilke et al. (2005)]. They have the following starting composition: 14.38 ± 0.21 wt% FeO, 47.88 ± 0.20 wt% $SiO_2$, 13.22 ± 0.16 wt% $Al_2O_3$, 9.04 ± 0.08 wt% CaO, 4.68 ± 0.08 wt% $Na_2O$, 4.04 ± 0.10 wt% $TiO_2$ and 3.23 ± 0.06 wt% MgO. Their $Fe^{3+}/\sum Fe$ were determined by wet chemistry analysis and Mössbauer spectroscopy to 0.83±0.04 (RB0-1) and 0.16±0.04 (Rb0-4). In addition, we studied an Fe-doped haplogranitic glass synthesized in air at 1600°C (AOQ-2, 8.4 ± 0.2 wt% $Fe_2O_3$, 72.9 ± 0.5 wt% $SiO_2$, 10.8 ± 0.2 wt% $Al_2O_3$, 4.5 ± 0.1 wt% $K_2O$ and 3.4 ± 0.2 wt% $Na_2O$). A $Fe^{3+}/\sum Fe$ of 0.63±0.04 was determined by Mössbauer spectroscopy (for experimental details see e.g. [Woodland and Jugo (2012)]). All glass samples were checked by optical polarization microscopy and with the EMP, so that occurrence of crystals is excluded. For XRS, the same glass batch was used as for Mössbauer spectroscopy.

### 3.2 Experiments

XRS spectra were acquired at 4 different experimental stations. In order to study the $q$-dependence of the Fe $M_{2/3}$-edge spectra, FeO ($Fe^{2+}$) and $\alpha$-$Fe_2O_3$ ($Fe^{3+}$), both octahedrally coordinated, were measured at beamline PNC/XSD 20-ID of the Advanced Photon Source (APS) employing the LERIX spectrometer [Fister et al. (2006)]. Here, 19 Si analyzer crystals are arranged on a semicircle with a radius of 1 m for vertical scattering geometry covering the scattering angles from 9° to 171°, which corresponds to $q$ between 0.8 $Å^{-1}$ to 10.0 $Å^{-1}$. The Si(555) reflection was used with an analyzer energy of 9.89 keV. The incident energy was monochromatized by a Si(111)-monochromator and an overall energy resolution of 1.5 eV was achieved. The $M_{2/3}$-edges were measured for energy-loss values between 45 eV to 70 eV by variation of the incident energy. At beamline ID16 of the European Synchrotron Radiation Facility (ESRF), measurements of the Fe $M_{2/3}$-edges of $Fe_2O_3$, $Fe_2SiO_4$, $FePO_4$, and $FeAl_2O_4$ were performed using the multiple element spectrometer for non-resonant inelastic x-ray spectroscopy of electronic excitations [Verbeni et al. (2009)], both for low and high $q$. The analyzer energy was set to 9.69 keV using the Si(660)-reflection and an overall energy resolution of 0.8 eV was obtained employing the Si(111) pre-monochromator together with a Si(220) channel-cut monochromator [Honkanen et al. (2013)]. Here, XRS spectra were collected utilizing a 9 analyzer array positioned at average scattering angles of 30° and 130° corresponding to $q$ of 2.05 $Å^{-1}$ and 9.1 $Å^{-1}$, respectively. The iron $M_{2/3}$-edges of iron bearing glasses were measured using the inelastic x-ray scattering spectrometer of beamline P01 at PETRA III (DESY), which is similar to that reported in [Verbeni et al. (2009)] but with vertical scattering plane and 5 Si(660) analyzer crystals. A total energy resolution of 0.6 eV was achieved utilizing a Si(311) monochromator. Here, the average scattering angle was 135° corresponding to a momentum transfer of 9.1 $Å^{-1}$. Preliminary studies of the $M_{2/3}$- and L-edges of FeO, $Fe_2SiO_4$ and $\alpha$-$Fe_2O_3$ using XRS were conducted at beamline BL12XU of SPring8 [Cai et al. (2004)] to prove the feasibility of an XRS $M_{2/3}$-edge study for the analysis of iron bearing minerals.

In all experiments several subsequent spectra were measured and summed up for each analyzer. The spectra were background corrected and finally normalized to the integral intensity between 49 eV and 68 eV energy loss. To increase the statistical accuracy, XRS spectra measured for similar $q$ were added if the $q$-dependence was found to be weak, which will be discussed in more detail in the next section. For low $q$, spectra obtained by 2 analyzers with the same momentum transfer could be summed up. At high $q$, spectra of all analyzers could be summed, which significantly enhances the statistical accuracy. This way of data processing was applied only for the experiments using the ID16 and P01 setup, whereas for data collected using the LERIX spectrometer each analyzer crystal was treated separately to determine the

$q$-dependence of the spectra.

The procedures applied to separate the Fe $M_{2/3}$-edge from the particle-hole excitation spectrum and Compton background for low and high $q$, respectively, is similar to those reported by [Sternemann et al. (2008)]. For low $q$, the Fe $M_{2/3}$-edge can be found on the tail of the particle-hole excitation spectrum with its maximum at lower energy loss than the edge. Here, a Pearson function or likewise a Gaussian or a Lorentzian function can be used to approximate the underlying background (see figure 1 a)). With increasing $q$ the particle-hole excitation spectrum transforms to the Compton spectrum. The maximum of the Compton peak moves to higher energy loss. This makes the subtraction of the Compton background difficult if the Compton maximum appears in the vicinity of the Fe $M_{2/3}$-edge. Here, one can use either a Gaussian to approximate the Compton peak shape [Fister et al. (2009)] or the extraction procedure described in [Sternemann et al. (2008)]. For high $q$ the Compton peak is located at much higher energy loss than the Fe $M_{2/3}$-edge, so that it lies on a smoothly increasing background, which can be modeled as discussed for low $q$ or, alternatively, by a linear fit (see figure 1 b)). As indicated in figure 1, different modeling of background does not significantly influence the shape of the Fe $M_{2/3}$-edge as long as energy-loss values up to 15 eV above the edge onset are considered. For the data of the LERIX spectrometer, we used a Gaussian for background subtraction throughout the whole $q$-range, whereas for ESRF data a Lorentzian and a linear background was used for low and high $q$, respectively.

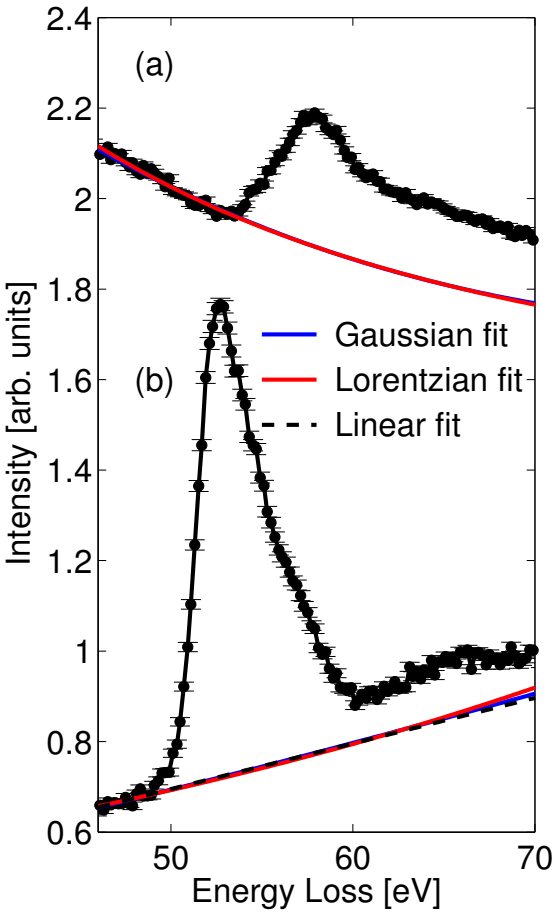


**Fig. 1** Different background subtraction procedures shown on the example of the Fe $M_{2/3}$-edges (black) measured at selected momentum transfer values of (a) 1.57 Å$^{-1}$ and (b) 7.62 Å$^{-1}$. For low $q$, the Fe $M_{2/3}$-edge is found on the high energy-loss tail of the particle-hole excitation spectrum. At high $q$, the Fe $M_{2/3}$-edge appears on the low energy-loss tail of the Compton peak.

## 4 Momentum transfer dependence of the Fe $M_{2/3}$-edge

The $q$-dependence of XRS spectra of the $M_{2/3}$-edge of octahedrally coordinated Fe in FeO ($Fe^{2+}$) and $\alpha$-$Fe_2O_3$ ($Fe^{3+}$) is presented in figure 2 a)-c) for a large $q$-range between 0.8 to 10.0 Å$^{-1}$. For $q < 2$ Å$^{-1}$ in the dipole limit ($k$=1, see equation 3), clear spectral differences between $Fe^{2+}$ and $Fe^{3+}$ are observed in the energy-loss region from 54 eV to 60 eV. Here, the spectra of $Fe_2O_3$ show only one broad maximum at 58 eV, whereas the spectra of FeO show an additional shoulder at 55 eV. Both spectra exhibit a relatively high edge step for energy-loss values above 63 eV due to excitations into continuum states. With increasing $q$ the spectral shape changes significantly due to the increasing contribution of octupole ($k$=3) transitions to the excitation spectrum and only small contributions by continuum excitations. This is most prominently manifested by an intensity increase for energy-loss values below 55 eV. Finally, the spectral q-dependent changes are found to be weak for $q > 8$ Å$^{-1}$ and the spectra show an asymmetric shape with a maximum at 52 eV and a shoulder at higher energy loss in the case of $Fe^{2+}$. For $Fe^{3+}$, only a single maximum at 53.5 eV is observed.

The experimental results are compared with calculations employing an atomic multiplet code [de Groot (2005), de Groot (2008)] (see Fig. 2). The multiplet calculations were performed using the modified CTM4XAS package [Stavitski and de Groot (2010)] to obtain Fe absorption edges similar to the model used by van der Laan [van der Laan (1991)] for dipole and octupole transitions. Continuum excitations are not considered in the theoretical approach. To calculate the $M_{2/3}$-edge, the values for the crystal-field splitting found in [de

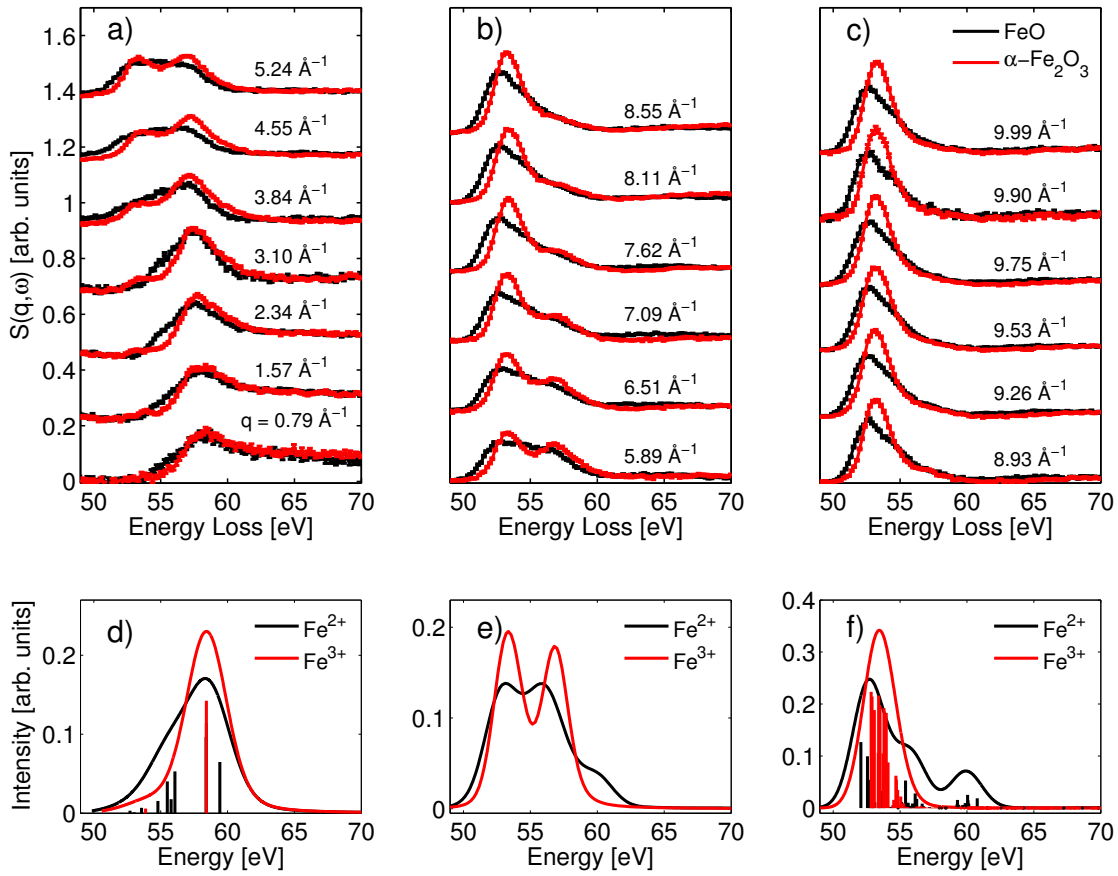


**Fig. 2** Upper panel: The effect of momentum transfer on the Fe $M_{2/3}$-edge for octahedrally coordinated $Fe^{2+}$ (FeO) and $Fe^{3+}$ ($\alpha$-$Fe_2O_3$) in the $q$ ranges 0.8-5.2 Å$^{-1}$ (a), 5.9-8.5 Å$^{-1}$ (b), and 8.9-10 Å$^{-1}$ (c). Lower panel: multiplet calculations for the dipole (d) and octupole (f) contribution as well as a 1:1 superposition of both to model the intermediate $q$-range (e).

Groot et al. (2005)] have been used. For a better agreement with the data, the Slater-Condon parameters were reduced to 64% of their atomic value and no spin-orbit splitting was applied. The calculated transition patterns were convoluted with a Lorentzian function (FWHM of 0.6 eV [Fuggle and Alvarado (1980)]) and with a Gaussian function (FWHM of 1.5 eV) to simulate the natural broadening of the states and the experimental resolution, respectively. In figure 2 d), calculations in the dipole limit (low q, $k$=1) are shown and are compared to results considering only octupole transitions ($k$=3, high $q$ limit), see figure 2 f). The modeled spectra resemble adequately both the spectral differences observed for the different oxidation states of iron and the $q$-dependence of the experiment although the weak maximum of the calculated $Fe^{2+}$ spectrum at high $q$ is not present in the measurement. Notably, for high $q$ the excitation spectra are dominated by octupole transitions with only small contribution by the continuum excitations. The spectrum of the dipole excitations appears broader compared to that of the octupole excitations. This may be explained by its higher energy position allowing its interaction with excitations into the continuum states [Sen Gupta et al. (2011), Sahle et al. (2014)]. The XRS measurements in the crossover regime, e.g. at $q$ = 5.89 Å$^{-1}$, can be properly reproduced by a superposition of dipole and octupole multiplet calculations with a 1:1 ratio (figure 2 e)).

The observed $q$-dependence has two major implications for the study of iron speciation by XRS spectroscopy: i) Both, experiment and theory indicate very strong spectral changes due to iron oxidation state, which is observed particularly well at high momentum transfers; ii) The $q$-dependence of the spectra for q > 8.11 Å$^{-1}$ is negligible. Consequently, spectra measured with different analyzers at different $q$ in the high $q$-limit can be summed up, which significantly increases the statistical accuracy of the experimental results. Hence, measure-

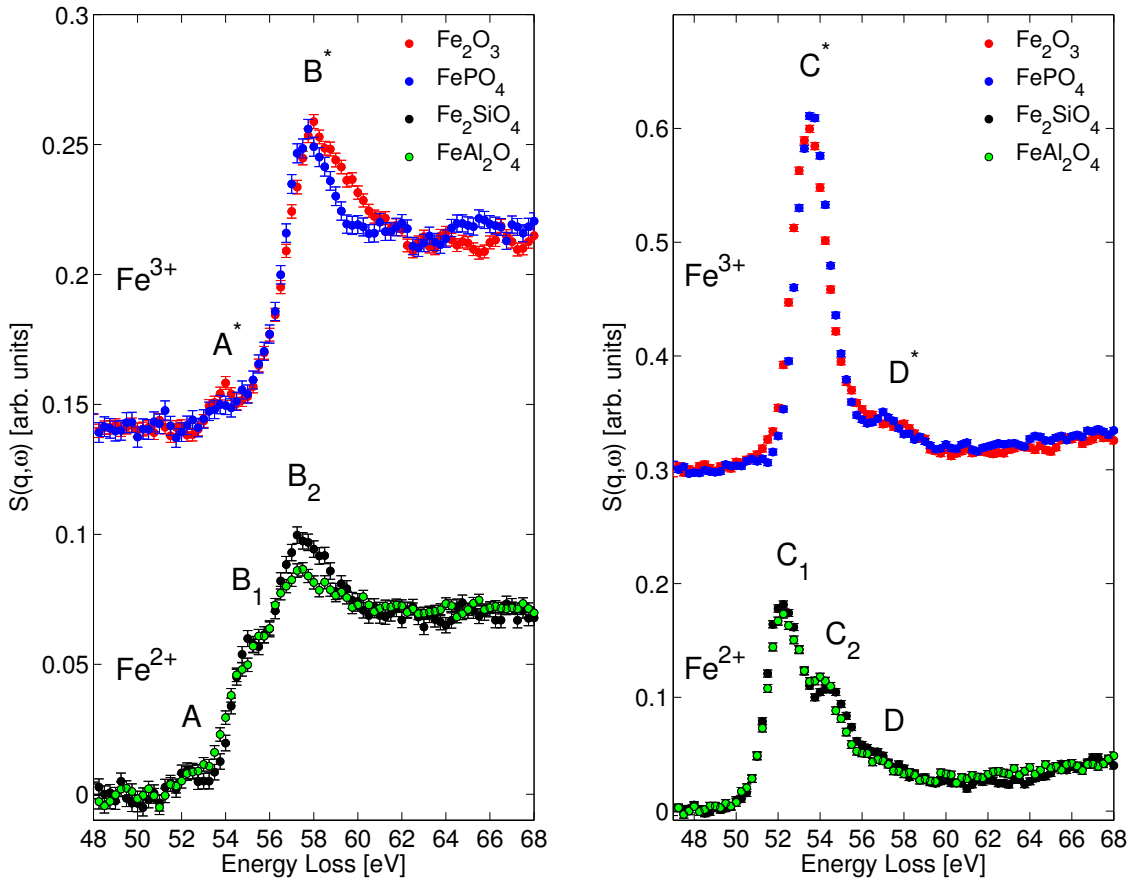


**Fig. 3** High resolution measurements of the Fe $M_{2/3}$-edge on $Fe^{2+}$ and $Fe^{3+}$ (both octahedral and tetrahedral) for q = 2.05 $Å^{-1}$ (left) and q = 9.1 $Å^{-1}$ (right), respectively. See text for detailed discussion.

ments at high $q$ in back-scattering geometry would be preferred to obtain high quality and decrease acquisition time.

## 5 Determination of the oxidation state and local coordination

In this section we discuss how oxidation state ($Fe^{2+}$, $Fe^{3+}$) and/or coordination (octahedral, tetrahedral) of iron change the shape of the Fe $M_{2/3}$-edge. For this comparison, we will use the spectra obtained at ID16. The XRS spectra of the four reference compounds measured at low $q$ in the dipole limit are presented in figure 3 (left). The spectrum of $\alpha$-$Fe_2O_3$ ($Fe^{3+}$, octahedral) shows a strong excitation peak at 58.0 eV (B*) and a weak pre-edge feature at 53.5 eV (A*). These features are similar to those observed by Xiong et al. [Xiong et al. (2012)] using SXAS. Excitations into continuum states cause the high intensity in the post edge region. When compared to the XRS spectrum of $FePO_4$ ($Fe^{3+}$, tetrahedral), the pre-edge intensity A* is broader and less pronounced, whereas a sharper main peak (B*) is observed. The edge onset for $FePO_4$ is slightly shifted to lower energy loss by 0.25 eV.

The XRS spectrum of $Fe_2SiO_4$ ($Fe^{2+}$, octahedral) is characterized by a two-peak structure with maxima at 54.5 eV and 57.3 eV ($B_1$ and $B_2$) together with a weak pre-edge feature at 52.8 eV (A). A comparison with the spectrum of $FeAl_2O_4$ ($Fe^{2+}$, 85% tetrahedral) yields a similar two peak spectral shape but the features $B_1$ and $B_2$ are broader and the edge onset is slightly shifted to higher energy by around 0.2 eV. Moreover, a less pronounced pre-peak intensity is observed in line with the findings for tetrahedral $Fe^{3+}$ in $FePO_4$ (berlinite structure). It must be recalled, that the $FeAl_2O_4$ sample contains 15% $Fe^{2+}$ in octahedral coordination [Andreozzi and Lucchesi (2002)], and this cation disorder might affects the spectral features slightly. Overall, small but

distinct differences due to local Fe coordination are found for both oxidation states.

In contrast, the difference of the spectra for the two oxidation states is striking (see also EELS measurements by van Aken [van Aken et al. (1999)] and calculations by van der Laan [van der Laan (1991)]). There is a large energy shift of 2.5 eV between the edge onsets of $Fe^{2+}$ and $Fe^{3+}$ with a remarkable difference in line shape, i.e. a double-peak structure of the $Fe^{2+}$ main edge in contrast to a single peaked $M_{2/3}$-edge for $Fe^{3+}$. These strong differences enable a separation between different Fe oxidation states and should allow for precise determination of the $Fe^{3+}/\sum Fe$.

At high $q$, the line shape and energy onset of the Fe $M_{2/3}$-edge changes completely. The XRS spectra of $Fe_2O_3$ and $FePO_4$ show a strong maximum ($C^*$) dominating the $M_{2/3}$-edge spectra at the energy-loss position, where the pre-peak is observed for low $q$. This difference is due to the dominating contribution of octupole transitions at high $q$. In contrast to low $q$, there is a slight energy shift of 0.25 eV for the edge onset to lower energy-loss values for the octahedral compared to the tetrahedral $Fe^{3+}$. The former also shows a less pronounced feature $D^*$, which is most probably due to small but still visible contributions from dipole excitations.

Concerning the $Fe^{2+}$ compounds at high $q$, the spectral shape of $FeAl_2O_4$ is very similar to that of $Fe_2SiO_4$. The typical double-peak structure is conserved but shifted as for $Fe^{3+}$ to lower energy loss and exhibits in contrast to low $q$ a more intense first peak at 52.3 eV ($C_1$) and a less pronounced second peak at 54.0 eV ($C_2$). We find the high energy-loss feature (D) to be broader and shifted to lower energy loss compared to $Fe^{3+}$ in accordance to the broader line shape and energy shift of $Fe^{3+}$ found at low $q$.

Between tetrahedrally and octahedrally coordinated $Fe^{2+}$ at high $q$, only subtle differences are found, i.e. a shift of the $C_2$ peak position to higher energy loss for octahedral coordination and a small variation in the intensity of peaks $C_1$ and $C_2$. This difference in intensity might be due to small contribution of $Fe^{3+}$ and to a less extent due to octahedral $Fe^{2+}$ contained in the $FeAl_2O_4$ sample as discussed below. Apparently the spectral differences with respect to the different oxidation states are at least as significant as observed for low $q$.

Our observations imply that the $M_{2/3}$-edge spectra enable to distinguish between tetrahedral and octahedral coordination, particularly with spectra obtained at low $q$. These relatively small differences between octahedrally and tetrahedrally coordinated Fe demand measurements of the $M_{2/3}$-edge with high statistical accuracy, particularly if the changes in pre-edge intensity are

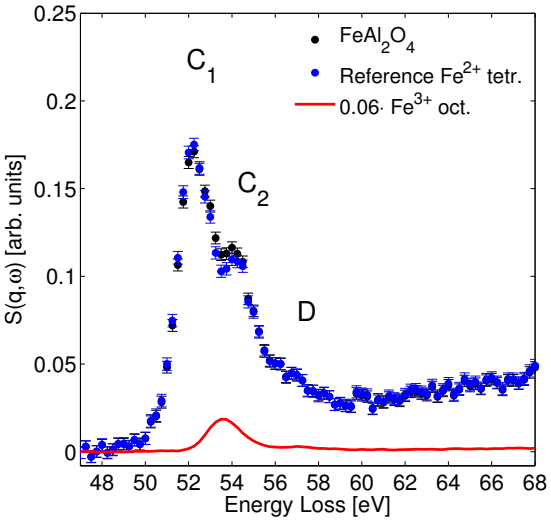


**Fig. 4** Spectra of $FeAl_2O_4$ before and after correction for 6% octahedral $Fe^{3+}$ contained in this sample. The corrected spectrum is used as reference for tetrahedral $Fe^{2+}$. Shown in red is the spectrum $Fe_2O_3$ weighted by 0.06 that was subtracted from the original $FeAl_2O_4$ spectrum.

to be employed. We would like to note, however, that the use of pre-peak shape and intensity in the analysis of local coordination might be not straightforward. E.g. Xiong et al. [Xiong et al. (2012)] found significant changes in the pre-peak for octahedrally coordinated $Fe^{3+}$ in $FePO_4{\cdot}2H_2O$ compared to that in $\alpha$-$Fe_2O_3$. These differences are related to the distortion of the octahedra in $FePO_4{\cdot}2H_2O$ with respect to the regular ones in $Fe_2O_3$.

To use these XRS spectra as references for characterizing $Fe^{3+}/\sum Fe$ of unknown samples requires references with pure $Fe^{2+}$ and $Fe^{3+}$ oxidation states. As the $FeAl_2O_4$ sample contains about 6% $Fe^{3+}$ at octahedral sites [Andreozzi and Lucchesi (2002)], it was corrected for the $Fe^{3+}$ contribution by subtracting the XRS spectrum of $Fe_2O_3$ weighted by 0.06. After subtraction, the resulting spectrum was normalized according to the procedure discussed above. The correction scheme is presented in figure 4 for the high $q$ measurement. The corrected XRS spectrum conserves the peak shift of structure $C_2$ but the intensity ratio of peaks $C_1$ and $C_2$ changes slightly, being now closer to the ratio found for $Fe_2SiO_4$. A correction of the $FeAl_2O_4$ spectrum for 15 % octahedrally coordinated $Fe^{2+}$ can be disregarded due to the similar shape of tetrahedral and octahedral $Fe^{2+}$ XRS spectra.

Overall the spectra measured at high $q$ show a much better statistical accuracy as we were able to sum up spectra acquired with several analyzer crystals, which

is advantageous in the analysis of oxidation state and coordination of an unknown sample.

## 6 Determination of $Fe^{3+}/\sum Fe$

In this section we explore the possibility of using the Fe $M_{2/3}$-edge for determining the Fe oxidation state in minerals and compounds. In the light of the many techniques already available, we would like to point out that the $M_{2/3}$-edge measured by XRS may provide a substantially improved way of obtaining this information particularly in experiments performed in-situ at high pressure and temperature. Here, we aim at evaluating the technique for extracting the $Fe^{3+}/\sum Fe$ in terms of procedure and precision. For doing so, we present measurements of the Fe $M_{2/3}$-edge on iron-containing glasses with $Fe^{3+}/\sum Fe$ ratios ranging from about 0.1 to 0.9. We used spectra collected at high momentum transfer. The XRS spectra of the glasses were measured with slightly better energy resolution than the reference samples. To match the energy resolution of both experiments for the fitting procedure, the spectra of the glasses were artificially broadened by a convolution with a Gaussian of 0.6 eV FWHM.

The spectra of the glasses are presented in figure 5. The Fe $M_{2/3}$-edge of the RB0-4 glass (right) shows a shape similar to those of $Fe_2SiO_4$ or $FeAl_2O_4$. In contrast, the spectra of the AOQ-2 and RB0-1 glasses show shapes very similar to that of $Fe^{3+}$-oxide. It is noted that due to the strong multiplet excitations, contributions from other light elements contained in the samples do not influence the Fe $M_{2/3}$-edge spectrum significantly. This is evidenced by the Mg-bearing RB0-glasses for the Mg L-edge, which is located in the same energy range as the Fe $M_{2/3}$-edge.

For a quantitative analysis of the individual glasses, a superposition of $Fe^{2+}$ and $Fe^{3+}$ reference XRS spectra was fitted to the glass spectra. Here, three different sets of fits were performed. For the first fit, (I) spectra of octahedral $Fe^{2+}$ and $Fe^{3+}$ references ($Fe_2SiO_4$ and $Fe_2O_3$) were used (blue line). For the second fit (II), $FeAl_2O_4$ and $FePO_4$ (both tetrahedral iron coordination) were used to investigate the influence of the coordination (red line). In silicate glasses, the Fe coordination shows site-to-site distribution with variable distortion or even mixed coordination. Hence, the use of spectra of crystalline samples with only one sort of coordination might not be appropriate. In order to analyze this, a weighted sum of all four reference spectra ($Fe^{2+}$ and $Fe^{3+}$, both octahedral and tetrahedral) was fitted to the glass spectra (III). For fitting procedures (II) and (III) we used the $FeAl_2O_4$ XRS spectrum corrected for the $Fe^{2+}$ contribution (c.f. figure 4).

The results are shown in figure 5. The general shape of the edge is reproduced well by all three ways of fitting with reference spectra. However, the fit revealed by superposition of all four references (green line) shows the best agreement, especially in the case of RB0-4 (5, right).

The quantitative results obtained by the fitting procedures can be found in table 1. The resulting $Fe^{3+}/\sum Fe$ of the glasses extracted by a fit of $Fe^{2+}$ and $Fe^{3+}$ reference spectra for octahedral coordination tend to overestimate the $Fe^{3+}/\sum Fe$ compared to the results revealed by Mössbauer spectroscopy. While the $Fe^{3+}/\sum Fe$ of the RB0-glasses measured by XRS are close to the Mössbauer results, the deviation becomes very significant in the case of the AOQ-2 glass. Using $FePO_4$ (tetrahedral coordination) as reference for $Fe^{3+}$ significantly affects the results. Here, a better agreement is found for the AOQ-2 glass but the $Fe^{3+}/\sum Fe$ of the RB0-glasses are underestimated. Thus, we conclude that the effect of coordination cannot be neglected in the fitting procedure although the spectra show only subtle differences as discussed before. The $Fe^{3+}$ fraction of the RB0-1 glass seems to have predominantly octahedral coordination, while the tetrahedral coordination is preferred for the $Fe^{3+}$ contribution in the AOQ-2 glass. To quantify this effect, the fitting procedure (III) was used with all four reference spectra to determine not only the $Fe^{3+}/\sum Fe$ ratio but also the contribution of a certain coordination. This procedure reveals an improved agreement between the measured and fitted spectra of all glasses. Octahedral coordination is preferred for $Fe^{2+}$ in all samples, while the fraction of tetrahedral $Fe^{2+}$ can be neglected. In contrast, both octahedral and tetrahedral coordinations of $Fe^{3+}$ contribute to the spectra for all samples, especially those with high $Fe^{3+}/\sum Fe$ ratio. The RB0-1 glass seems to contain slightly more octahedral $Fe^{3+}$ than tetrahedral $Fe^{3+}$, while the AOQ-2 glass tends to have more tetrahedral $Fe^{3+}$. Evidence for mixed coordination of Fe in silicate glasses has been already provided by various techniques (e.g. [Virgo and Mysen (1985), Drewitt et al. (2013), Farges et al. (2004), Wilke et al. (2005)]). In addition to mixtures of tetrahedral and octahedral coordination, also the presence of fivefold coordination in trigonal bipyramidal symmetry has been proposed [Rossano et al. (1999), Galoisy et al. (2001), Jackson et al. (2005)]. The difference observed here for the two compositions is consistent to the trends observed using the pre-edge of the Fe K-edge XANES [Farges et al. (2004), Wilke et al. (2005), Wilke et al. (2007)], that were interpreted as evidence that the coordination of $Fe^{3+}$ is considerably influenced by the polymerization of the melt. Despite the similarity in the results, we would like to stress here that Fe $M_{2/3}$-

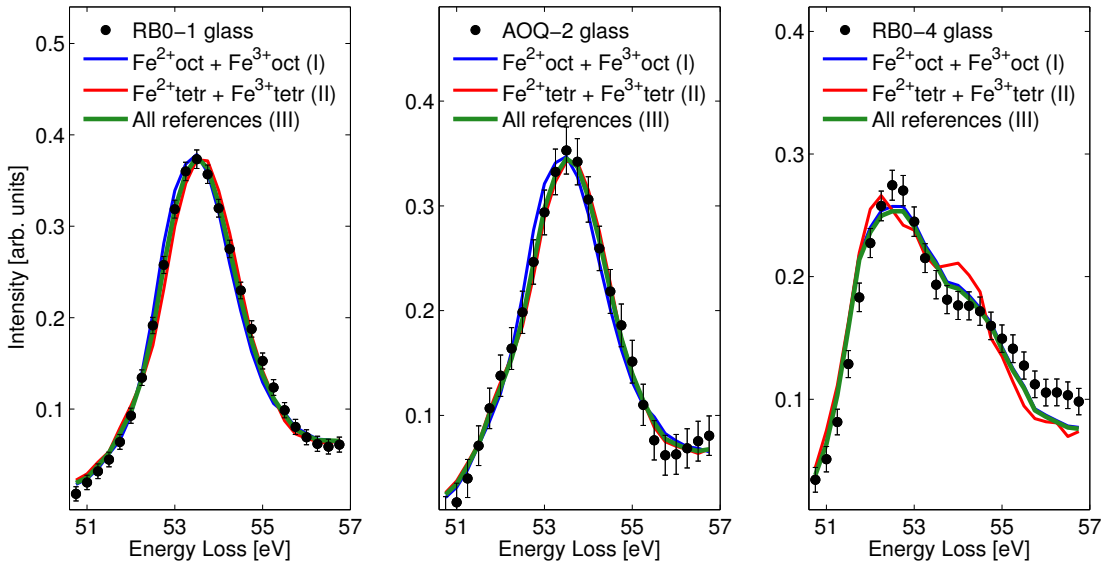


**Fig. 5** Fe $M_{2/3}$-edge spectra of glasses with different $Fe^{3+}/\sum Fe$ shown together with the results of the fits employing different reference spectra (see text for details).

| | RB0-1 | AOQ-2 | RB0-4 |
|---|---|---|---|
| $Fe^{3+}/\sum Fe$ XRS (I) | 0.89±0.01 ($R^2$=0.9890) | 0.73±0.04 ($R^2$=0.9780) | 0.18±0.02 ($R^2$=0.9274) |
| $Fe^{3+}/\sum Fe$ XRS (II) | 0.74±0.05 ($R^2$=0.9884) | 0.61±0.04 ($R^2$=0.9880) | 0.14±0.04 ($R^2$=0.8561) |
| $Fe^{3+}/\sum Fe$ XRS (III) | 0.82±0.03 ($R^2$=0.9964) | 0.69±0.05 ($R^2$=0.9911 | 0.18±0.01 ($R^2$=0.9291) |
| $Fe^{3+}/\sum Fe$ Mössbauer | 0.83±0.04 | 0.63±0.04 | 0.16±0.04 |

**Table 1** Comparison of the $Fe^{3+}/\sum Fe$ for different glasses using the fitting procedures (I), (II), and (III) with results obtained by Mössbauer spectroscopy. The coefficient of determination $R^2$ quantifies the agreement between the experimental data and the different fitting procedures.

edges with improved statistics are required to conduct a reliable analysis of the average coordination number of iron in glasses. Still, this preliminary result is particularly exciting, as this method would not only allow determining the iron oxidation state at in-situ conditions but also detecting coordination changes as a function of pressure and/or temperature, hardly feasible by any other method.

## 7 Conclusion

In this paper we demonstrated the capabilities of XRS spectroscopy to study the $M_{2/3}$-edge of iron in different iron bearing minerals and compounds and showed how XRS spectra can be used to reveal information about the oxidation state and the local coordination of iron. The determination of the $Fe^{3+}/\sum Fe$ can be performed with high sensitivity due to the strong spectral changes observed at the Fe $M_{2/3}$-edge. Our data provide strong evidence that estimation of iron coordination of $Fe^{2+}$ and $Fe^{3+}$ in glasses or even melt is feasible. We showed that the $q$-dependence of the XRS spectra can be used to tune the sensitivity of the measurements. Because XRS is a bulk probe, Fe $M_{2/3}$-edge studies, which have been restricted to vacuum conditions so far, can now be conducted on samples that are incompatible with vacuum or even in experiments at high pressure and high temperature using e.g. a resistively or laser heated DAC. Thus, XRS provides an exciting tool to study the coordination, oxidation state and even the spin state [Nyrow et al., to be published] of iron in minerals, glasses and melts at conditions relevant for the Earth's interior and gives access to unique complementary information on iron speciation at in-situ conditions for many geophysical and geochemical applications.

**Acknowledgements** We acknowledge ESRF, APS, SPring-8 and DELTA for providing synchrotron radiation. AN and KM would like to thank BMBF (05K10PEC) for financial support. JST and RAG acknowledge the support from NSERC of Canada (MFA, Discover grant). The authors would also like to thank M. Stuff and D. Rhede (GFZ) for the electron microprobe analysis of the AOQ-2 sample and J. Pohlenz for proof-reading.

## References


[Andreozzi and Lucchesi (2002)] Andreozzi GB, Lucchesi S: Intersite distribution of $Fe^{2+}$ and Mg in the spinel (sensu stricto)-hercynite series by single-crystal X-ray diffraction. Amer. Min. **87**:1113–1120 (2002)

[Antonangeli et al. (2010)] Antonangeli D, Siebert J, Badro J, Farber DL, Fiquet G, Morard G, Ryerson FJ: Composition of the Earth's inner core from high-pressure sound velocity measurements in Fe-Ni-Si alloys. Earth and Planetary Science Letters **295**, 292–296 (2010)

[Badro et al. (2003)] Badro J, Fiquet G, Guyot F, Rueff JP, Struzhkin VV, Vanko G, Monaco G: Iron Partitioning in Earth's Mantle: Toward a Deep Lower Mantle Discontinuity. Science **300**, 789–791 (2003)

[Bergmann et al. (2004)] Bergmann U, Groenzin H, Mullins OC, Glatzel P, Getzer J, Cramer SP: X-Ray Raman Spectroscopy: A New Tool to Study Local Structure of Aromatic Hydrocarbons and Asphaltenes. Petroleum Science and Technology **22**, 863–875 (2004)

[Berry et al. (2010)] Berry AJ, Yaxley GM, Woodland AB, Foran GJ: A XANES calibration for determining the oxidation state of iron in mantle garnet. Chemical Geology **278**, 31–37 (2010)

[Boulard et al. (2012)] Boulard E, Menguy N, Auzende AL, Benzerara K, Bureau H, Antonangeli D, Corgne A, Morard G, Siebert J, Perrillat JP, Guyot F, Fiquet G: Experimental investigation of the stability of Fe-rich carbonates in the lower mantle. Journal of Geophysical Research **117**, B02208 (2012)

[Bourdelle et al. (2013)] Bourdelle F, Benzerara K, Beyssac O, Cosmidis J, Neuville DR, Brown GE Jr, Paineau E: Quantification of the ferric/ferrous iron ratio in silicates by scanning transmission X-ray microscopy at the Fe $L_{2,3}$ edges. Contrib. Mineral. Petrol. **166**, 423-434 (2013)

[Bradley et al. (2011)] Bradley JA, Moore KT, van der Laan G, Bradley JP, Gordon RA: Core and shallow-core d- to f-shell excitations in rare-earth metals. Phys. Rev. B **84**, 205105 (2011)

[Cai et al. (2004)] Cai YQ, Chow P, Chen CC, Ishii H, Tsang L, Kao CC, Liang KS, Chen CT: Optical Design and Performance of the Taiwan Inelastic X-Ray Scattering Beamline (BL12XU) at SPring-8. AIP Conf. Proc. **705**, 340–343 (2004)

[Calvert et al. (2005)] Calvert CC, Brown A, Brydson R: Determination of the local chemistry of iron in inorganic and organic materials. Journal of Electron Spectroscopy and Related Phenomena **143**, 173–187 (2005)

[Cavé et al. (2006)] Cavé L, Al T, Loomer D, Cogswell S, Weaver L. A STEM/EELS method for mapping iron valence ratios in oxide minerals. Micron **37**, 301–309 (2006)

[Crocombette et al. (1995)] Crocombette JP, Pollak M, Jollet F, Thromat N, Gautier-Soyer M: X-Ray Near-Edge Absorption Study of Temperature-Induced Low-Spin-to-High-Spin Change in Metallo-Supramolecular Assemblies. Phys. Rev. B **52**, 3143–3150 (2006)

[de Groot (2005)] de Groot FMF: Multiplet effects in X-ray spectroscopy. Coordination Chemistry Reviews **249**, 31–63 (2005)

[de Groot et al. (2005)] de Groot FMF, Glatzel P, Bergmann U, van Aken PA, Barrea RA, Klemme S, Hävecker M, Knop-Gericke A, Heijboer WM, Weckhuysen BM: 1s2p Resonant Inelastic X-ray Scattering of Iron Oxides. J. Phys. Chem. B **109**, 20751–20762 (2005)

[de Groot (2008)] de Groot FMF: Ligand and metal X-ray absorption in transition metal complexes. Inorganica Chemica Acta **361**, 850–856 (2008)

[de Groot et al. (2010)] de Groot FMF, de Smit E, van Schooneveld MM, Aramburo LR, Weckhuysen BMX: In-situ Scanning Transmission X-Ray Microscopy of Catalytic Solids and Related Nanomaterials. Chem. Phys. Chem. **11**, 951–962 (2008)

[Ding et al. (2014)] Ding Y, Chen, CC, Zeng Q, Kim, HS, Han MJ, Balasubramanian M, Gordon R, Li F, Bai L, Popov D, Heald SM, Gog T, Mao H, van Veenendaal M: Novel High-Pressure Monoclinic Metallic Phase of V2O3. Phys. Rev. Lett. **112**, 056401 (2014)

[Drewitt et al. (2013)] Drewitt JE, Sanloup C, Bytchkov A, Brassamin S, Hennet L: Structure of $(Fe_xCa_{1-x}O)_y(SiO_2)_{1-y}$ liquids and glasses from high-energy x-ray diffraction: Implications for the structure of natural basaltic magmas. Physical Review B **87**, 224201 (2013)

[Duffy (2008)] Duffy TS: Mineralogy at the extremes. Nature **451**, 269–270 (2013)

[Dunlap et al. (1998)] Dunlap RA, Edelman DA, Mackay GR: A Mössbauer effect investigation of correlated hyperfine parameters in natural glasses (tektites). Journal of Non-Crystalline Solids **223**, 141–146 (1998)

[Edwards et al. (2000)] Edwards C, Bond PL, Druschel GK, McGuire MM, Hamers RJ, Banfield JFX: Geochemical and biological aspects of sulphide mineral dissolution: lessons from Iron Mountain, California. Chemical Geology **169**, 383–397 (1998)

[Fang and Ahuja (2008)] Fang C, Ahuja R: Local structure and electronic spin transition of Fe-bearing $MgSiO_3$ perovskite under conditions of the Earth's lower mantle. Physics of the Earth and Planetary Interiors **166**, 77–82 (2008)

[Farges et al. (2004)] Farges F, Lefrere Y, Rossano S, Berthereau A, Calas G, Brown GE Jr.: The effect of redox state on the local structural environment of iron in silicate glasses: a combined XAFS spectroscopy, molecular dynamics, and bond valence study. Journal of Non-crystalline Solids **344**, 176–188 (2004)

[Fierro et al. (2011)] Fierro G, Moretti G, Ferraris G, Andreozzi GB: A Mössbauer and structural investigation of Fe-ZSM-5 catalysts: Influence of Fe oxide nanoparticles size on the catalytic behaviour for the NO-SCR by $C_3H_8$. Applied Catalysis B: Environmental **102**, 215–223 (2011)

[Fister et al. (2006)] Fister TT, Seidler GT, Wharton L, Battle AR, Ellis TB, Cross JO, Macrander AT, Elam WT, Tyson TA, Qian Q: Multielement spectrometer for efficient measurement of the momentum transfer dependence of inelastic x-ray scattering. Review of scientific instruments **77**, 063901 (2006)

[Fister et al. (2009)] Fister TT, Magle KP, Vila FD, Seidler GT, Hamner C, Cross JO, Rehr JJ: Intermediate-range order in water ices: Nonresonant inelastic x-ray scattering measurements and real-space full multiple scattering calculations. Phys. Rev. B **79**, 174117 (2009)

[Fuggle and Alvarado (1980)] Fuggle JC, Alvarado SF: Core-level lifetimes as determined by x-ray photoelectron spectroscopy measurements. Phys. Rev. A **22**, 1615–1624 (2006)

[Galoisy et al. (2001)] Galoisy L, Callas G, Arrio MA: High-resolution XANES spectra of iron in minerals and glasses: structural information from the pre-edge region. Chemical Geology **174**, 307–319 (2001)

[Gauthier et al. (1999)] Gauthier C, Sole VA, Signorato R, Goulon J, Moguiline E: The ESRF beamline ID26: X-ray absorption on ultra dilute sample. Journal of Synchrotron Radiation **6**, 164–166 (1999)

[Gordon et al. (2008)] Gordon RA, Seidler GT, Fister TT, Haverkort MW, Sawatzky GA, Tanaka A, Sham TK: High multipole transitions in NIXS: Valence and hybridization in 4f systems. EPL **81**, 26004 (2008)

[Gordon et al. (2009)] Gordon RA, Haverkort MW, Sen Gupta S, Sawatzky GA: Orientation-dependent x-ray Raman scattering from cubic crystals: natural linear dichroism in MnO and $CeO_2$. Journal of Physics: Conference Series **190**, 012047 (2009)

[Hämäläinen and Manninen (2001)] Hämäläinen K, Manninen S: Resonant and non-resonant inelastic x-ray scattering. J. Phys.: Cond. Mat. **13**, 7539–7555 (2001)

[Haverkort et al. (2007)] Haverkort M W, Tanaka A, Tjeng LH and Sawatzky GA: Nonresonant Inelastic X-Ray Scattering Involving Excitonic Excitations: The Examples of NiO and CoO. Phys. Rev. Lett. **99**, 257401 (2007)

[Heijboer et al. (2005)] Heijboer WM, Koningsberger DC, Weckhuysen BM, de Groot FMF: New frontiers in X-ray spectroscopy in heterogeneous catalysis: Using Fe/ZSM-5 as test-system. Catalysis Today **110**, 228–238 (2005)

[Hofmeister (2006)] Hofmeister AM: Is low-spin $Fe^{2+}$ present in Earth's mantle?. Earth and Planetary Science Letters **243**, 44–52 (2006)

[Honkanen et al. (2013)] Honkanen AP, Verbeni R, Simonelli L, Moretti Sala M, Monaco G, Huotari S: Study on the reflectivity properties of spherically bent analyser crystals. J. Synch. Rad. **21**, 104–110 (2013)

[Inkinen et al. (2013)] Inkinen J, Sakko A, Ruotsalainen KO, Pylkkänen T, Niskanen J, Galambosi S, Hakala M, Monaco G, Huotari S, Hämäläinen K: Temperature dependence of CO2 and N2 core-electron excitation spectra at high pressure. Phys. Chem. Chem. Phys. **15**, 9231–9238 (2013)

[Irifune and Isshiki (1998)] Irifune T, Isshiki M: Iron partitioning in a pyrolite mantle and the nature of the 410-km seismic discontinuity. Nature **392**, 702–705 (1998)

[Jackson et al. (2005)] Jackson WE, Farges F, Yeager M, Mabrouk PA, Rossano S, Waychunas GA, Solomon EA, Brown GE Jr.: Multi-spectroscopic study of Fe(II) in silicate glasses: Implications for the coordination environment of Fe(II) in silicate melts. Geochimica and Cosmochimica Acta **69**, 4315–4332 (2005)

[Krisch and Sette (2002)] Krisch M, Sette F: X-ray Raman scattering from low-Z materials. Surface Review and Letters **9**, 969–976 (2002)

[Krywka et al. (2007)] Krywka C, Paulus M, Sternemann C, Volmer M, Remhof A, Nowak G, Nefedov A, Poter B, Spiegel M, Tolan M: The small-angle and wide-angle X-ray scattering set-up at beamline BL9 of DELTA. J. Synch. Rad. **14**, 244–251 (2007)

[Lee et al. (2005)] Lee SK, Eng PJ, Mao H-K, Meng Y, Newville M, Hu MY, Shu J: Probing of bonding changes in $B_2O_3$ glasses at high pressure with inelastic X-ray scattering. Nature Materials **4**, 851–854 (2005)

[Lee et al. (2008)] Lee SK, Lin J-F, Cai YQ, Hiraoka N, Eng PJ, Okuchi T, Mao H-K, Meng Y, Hu MY, Chow P, Shu J, Li B, Fukui H, Lee BH, Kim HN, Yoo C-S: X-ray Raman scattering study of $MgSiO_3$ glass at high pressure: Implication for triclustered $MgSiO_3$ melt in Earth's mantle. PNAS **105**, 7925–7929 (2008)

[Lin et al. (2010)] Lin J-F, Mao Z, Yavaş H, Zhao J, Dubrovinsky L: Shear wave anisotropy of textured hcp-Fe in the Earth's inner core. Earth and Planetary Science Letters **298**, 361–366 (2010)

[Mao et al. (2003)] Mao WL, Mao H-k, Eng PJ, Trainor TP, Newville M, Kao C-c, Heinz DL, Shu J, Meng Y, Hemley RJ: Bonding Changes in Compressed Superhard Graphite. Science **302**, 425–427 (2003)

[Mattila et al. (2005)] Mattila A, Soininen JA, Galambosi S, Huotari S, Vanko G, Zhigadlo ND, Karpinski J, Hämäläinen K: Local Electronic Structure of MgB2 by X-Ray Raman Scattering at the Boron K Edge. PRL **94**, 247003 (2005)

[McCammon (1997)] McCammon CA: Perovskite as a possible sink for ferric iron in the lower mantle. Nature **387**, 694–696 (1997)

[McCammon et al. (2004)] McCammon CA, Frost DJ, Smyth JR, Laustsen HMS, Kawamoto T, Ross NL, van Aken PA: Oxidation state of iron in hydrous mantle phases: implications for subduction and mantle oxygen fugacity. Physics of the Earth and Planetary Interiors **143-144**, 157–169 (2004)

[Miot et al. (2009)] Miot J, Benzerara K, Obst M, Kappler A, Hegler F, Schädler S, Bouchez C, GuyotF, Morin G: Extracellular Iron Biomineralization by Photoautotrophic Iron-Oxidizing Bacteria. Appl. Environ. Microbiol **75**(17), 5586–5591 (2009)

[Moreau et al. (2012)] Moreau P, Boucher F: Revisiting lithium K and iron $M_{2,3}$ edge superimposition: The case of lithium battery material $LiFePO_4$. Micron **43**, 16–21 (2012)

[Munoz et al. (2006)] Munoz M, De Andrade V, Vidal O, Lewin E, Pascarelli S, SusiniJ: Redox and speciation micromapping using dispersive X-ray absorption spectroscopy: Application to iron chlorite mineral of a metamorphic rock thin section, Geochem. Geophys. Geosyst. **7**, Q11020 (2006)

[Mysen (1991)] Mysen BO: Relations between structure, redox equilibria of iron, and properties of magmatic liquids. In Perchuk LL, Kushiro I, Eds., Advances in Physical Chemistry, **9**, 41–98 (1991)

[Narygina et al. (2009)] Narygina O, Mattesini M, Kantor I, Pascarelli S, Wu X, Aquilanti G, McCammon CA, Dubrovinsky L: High-pressure experimental and computational XANES studies of $(Mg,Fe)(Si,Al)O_3$ perovskite and (Mg,Fe)O ferropericlase as in the Earths lower mantle. Phys. Rev. B **79**, 174115 (2009)

[Newville et al. (1999)] Newville M, Sutton S, Rivers M, Eng P: Micro-beam X-ray absorption and fluorescence spectroscopies at GSECARS: APS beamline 13ID. Journal of Synchrotron Radiation **6**, 353–355 (1999)

[Nyrow et al., to be published] Nyrow A,Tse JS, Hiraoka N, Desgreniers S, Büning T, Mende K, Tolan M, Wilke M, Sternemann C, to be published (2014)

[Okuchi (1997)] Okuchi T: Hydrogen Partitioning into Molten Iron at High Pressure: Implications for Earths Core. Science **278**, 1781–1784 (1997)

[Ono et al. (2007)] Ono S, Ohishi Y, Kikegawa T: High-pressure study of rhombohedral iron oxide, FeO, at pressures between 41 and 142 GPa. J. Phys.: Condens. Matter **19**, 036205 (2007)

[Otsuka et al. (2010)] Otsuka K, McCammon CA, Karato S-I: Tetrahedral occupancy of ferric iron in (Mg,Fe)O: Implications for point defects in the Earth's lower mantle. Physics of the Earth and Planetary Interiors **180**, 179–188 (2010)

[Pacella et al. (2012)] Pacella A, Andreozzi GB, Fournier J, Stievano L, Giantomassi F, Lucarini G, Rippo MR, Pugnaloni A: Iron topochemistry and surface reactivity of amphibole asbestos: relations with in vitro toxicity. Anal Bioanal Chem. **402**(2), 871–881 (2012)

[Parkinson and Arculus (1997)] Parkinson IJ, Arculus RJ: The redox state of subduction zones: insights from arc-peridotites. Chemical Geology **160**, 409–423 (1997)

[Rossano et al. (1999)] Rossano S, Balan E, Morin G, Bauer JP, Calas G, Brouder C: $^{57}$Fe Mössbauer spectroscopy of tektites. Physics and Chemistry of Minerala **26**, 530-538 (1999)

[Sahle et al. (2013)] Sahle ChJ, Sternemann C, Schmidt C, Lehtola S, Jahn S, Simonelli L, Huotari S, Hakala M, Pylkkanen T, Nyrow A, Mende K, Tolan M, Hämäläinen K, Wilke M: Microscopic structure of water at elevated pressures and temperatures. PNAS **110**, 6301–6306 (2013)

[Sahle et al. (2014)] Sahle ChJ, Sternemann C, Sternemann H, Tse JS, Gordon RA, Desgreniers S, Maekawa S, Yamanaka S, Lehmkühler F, Wieland DCF, Mende K, Huotari S, Tolan M: The Ba 4d4f giant dipole resonance in complex Ba/Si compounds. J. Phys. B: At. Mol. Opt. Phys. **47**, 045102 (2014)

[Schmid et al. (2003)] Schmid R, Wilke M, Oberhänsli R, Janssens K, Falkenberg G, Franz L, Gaab A: Micro-XANES determination of ferric Iron and its application in thermobarometry. Lithos **70**, 381–392 (2003)

[Schülke (2007)] Schülke W: Electron Dynamics by Inelastic X-Ray Scattering. OUP Oxford Press (2007)

[Sen Gupta et al. (2011)] Sen Gupta S, Bradley JA, Haverkort MW, Seidler GT, Tanaka A, Sawatzky GA: Coexistence of bound and virtual-bound states in shallow-core to valence x-ray spectroscopies. PRB **84**, 075134 (2011)

[Smyth et al. (2005)] Smyth JR, Holl CM, Langenhorst F, Laustsen HMS, Rossmann GR, Kleppe A, McCammon CA, Kawamoto T, van Aken PA: Crystal chemistry of wadsleyite II and water in the Earth's interior. Physics and Chemistry of Minerals **31**, 691–705 (2005)

[Sobolev et al. (1999)] Sobolev VN, McCammon CA, Taylor LA, Snyder CA, Sobolev NV: Precise Moessbauer milliprobe determination of ferric iron in rock-forming minerals and limitations of electron microprobe analysis. Amer. Mineralogist **84**, 78–85 (1999)

[Soininen et al. (2005)] Soininen JA, Ankudinov AL, Rehr JJ: Inelastic scattering from core electrons: A multiple scattering approach. PRB **72**, 045136 (2005)

[Soininen et al. (2006)] Soininen JA, Mattila A, Rehr JJ, Galambosi S, Hämäläinen K: Experimental determination of the core-excited electron density of states. J. Phys.: Cond. Mat. **18**, 7327–7336 (2006)

[Stavitski and de Groot (2010)] Stavitski E, de Groot FMF: The CTM4XAS program for EELS and XAS spectral shape analysis of transition metal L edges. Micron **41**, 687–694 (2010)

[Sternemann et al. (2005)] Sternemann C, Soininen, JA, Huotari S, Vanko G, Volmer M, Secco RA, Tse JS, Tolan M: X-ray Raman scattering at the L edges of elemental Na, Si, and the N edge of Ba in Ba8Si46. PRB **72**, 035104 (2005)

[Sternemann et al. (2008)] Sternemann H, Sternemann C, Seidler GT, Fister TT, Sakko A, Tolan M: An extraction algorithm for core-level excitations in non-resonant inelastic X-ray scattering spectra. J. Synchrotron Rad. **15**, 162–169 (2008)

[Sternemann et al. (2013)] Sternemann C, Sahle ChJ, Mende K, Schmidt C, Nyrow A, Simonelli L, Moretti Sala M, Tolan M, Wilke M: X-ray Raman scattering: An exciting tool for the study of matter at conditions of the Earth's interior. Journal of Physics: Conference Series **425**, 202011 (2013)

[Tan et al. (2012)] Tan H, Verbeeck J, Abakumov A, Van Tendeloo G: Oxidation state and chemical shift investigation in transition metal oxides by EELS. Ultramicroscopy **116**, 24–33 (2012)

[Terasaki et al. (2011)] Terasaki H, Kamada S, Sakai T, Ohtani E, Hirao N, Ohishi Y: Liquidus and solidus temperatures of a Fe-O-S alloy up to the pressures of the outer core: Implication for the thermal structure of the Earth's core. Earth and Planetary Science Letters **304**, 559–564 (2011)

[Thy and Lofgren (1994)] Thy P, Lofgren GE: Experimental constraints on the low-pressure evolution of transitional and mildly alkalic basalts: the effect of Fe-Ti oxide minerals and the origin of basaltic andesites. Contrib. Mineral. Petrol **116**, 340–351 (1994)

[Tse et al. (2011)] Tse JS, Yang L, Zhang SJ, Jin CQ, Sahle ChJ, Sternemann C, Nyrow A, Giordano V, Jiang JZ, Yamanaka S, Desgreniers S, Tulk CA: Pressure-induced electron topological transitions in Ba-doped Si clathrate. Phys. Rev. B **84**, 184105 (2011)

[Tse et al. (2013)] Tse JS, Hanfland M, Flacau R, Desgreniers S, Li Z, Mende K, Gilmore K, Nyrow A, Moretti Sala M, Sternemann C: Electronic Structure and Electron Topology in the Direct fcc → sh Transformation of Silicon. J. Phys. Chem. C **118** 1161–1166 (2013)

[van Aken et al. (1999)] van Aken PA, Styrsa VJ, Liebscher B, Woodland AB, Redhammer GJ: Microanalysis of $Fe^{3+}/\sum Fe$ in oxide and silicate minerals by investigation of electron energy-loss near-edge structures (ELNES) at the Fe $M_{2,3}$ edge. Phys. Chem. Minerals **26**, 584–590 (1999)

[van der Laan (1991)] van der Laan G: $M_{2,3}$ absorption spectroscopy of 3d transition-metal compounds. J. Phys.: Cond. Mat. **3**, 7443 (1991)

[Verbeni et al. (2009)] Verbeni R, Pylkkänen T, Huotari S, Simonelli L, Vanko G, Martel K, Henriquet C, Monaco G: Multiple-element spectrometer for non-resonant inelastic X-ray spectroscopy of electronic excitations. J. Synchrotron Rad. **16**, 469–476 (2009)

[Virgo and Mysen (1985)] Virgo D, Mysen BO: The structural state of iron in oxidized vs. reduced glasses at 1 atm: a $^{57}$Fe Mössbauer study. Physics and Chemistry of Minerals **12**, 65-76 (1985)

[Westre et al. (1997)] Westre TE, Kennepohl P, DeWitt JG, Hedman B, Hodgson KO, Solomon EI: A Multiplet Analysis of Fe K-Edge 1s → 3d Pre-Edge Features of Iron Complexes. J. Am. Chem. Soc. **119** (27), 6297-6314 (1997)

[Wilke et al. (1999)] Wilke M, Behrens H: The dependence of the partitioning of iron and europium between plagioclase and hydrous tonalitic melt on oxygen fugacity. Contrib. Mineral Petrol. **137**, 102–114 (1999)

[Wilke et al. (2001)] Wilke M, Farges F, Petit P-E, Brown Jr GE, Martin F: Oxidation state and coordination of Fe in minerals: An Fe K-XANES spectroscopic study. Amer. Mineralogist **86**, 714–730 (2001)

[Wilke et al. (2005)] Wilke M, Partzsch GM, Bernhardt R, Lattard D: Determination of the iron oxidation state in basaltic glasses using XANES at the K-edge. Chemical Geology **220**, 143–161 (2005)

[Wilke et al. (2006)] Wilke M, Schmidt C, Farges F, Malavergne V, Gautron L, Simionovici S, Hahn M, Petit PE: Structural environment of iron in hydrous aluminosilicate glass and melt-evidence from X-ray absorption spectroscopy. Chemical Geology **229**, 144-161 (2006)

[Wilke et al. (2007)] Wilke M, Farges F, Partzsch GM, Schmidt C., Behrens H: Speciation of Fe in silicate glasses and melts by in-situ XANES spectroscopy. Amer. Min. **92**, 44–56 (2007)

[Wood et al. (1989)] Wood BJ, Virgo D: Upper mantle oxidation state: Ferric iron contents of Iherzolite spinels

by $^{57}$Fe Mssbauer spectroscopy and resultant oxygen fugacities. Geochimica et Cosmochimica Acta **53**, 691–705 (1989)

[Woodland and Jugo (2012)] Woodland AB, Jugo PJ: A complex magmatic system beneath the Devès volcanic field, Massif Central, France: evidence from clinopyroxene megacrysts. Contributions to Mineralogy and Petrology **153**(6), 719–731 (2012)

[Xiong et al. (2012)] Xiong W, Peng J, Hu Y: Use of X-ray absorption near edge structure (XANES) to identify physisorption and chemisorption of phosphate onto ferrihydrite-modified diatomite. J. Colloid Interface Sci. **368**, 528–532 (2012)

[Xu and Lin (2000)] Xu G, Lin X: Geology and geochemistry of the Changlongshan skarn iron deposit, Anhui Province, China. Ore Geology Reviews **16**, 91–106 (2000)

[Zerr and Boehler (1993)] Zerr A, Boehler R: Melting of (Mg, Fe)$SiO_3$-Perovskite to 625 Kilobars: Indication of a High Melting Temperature in the Lower Mantle. Science **262**, 553–555 (1993)

[Zerr and Boehler (1994)] Zerr A, Boehler R: Constraints on the melting temperature of the lower mantle from high-pressure experiments from MgO and magnesiowüstite. Nature **371**, 506–508 (1994)